Thermochemical Ablation of Ceramic Heat Shields

MARVIN B. ZIERING*
Avco Systems Division, Wilmington, Mass.

Simplified thermochemical ablation models are developed for three ceramic heat-shield materials, potentially useful as high-performance re-entry nosetips. The models are based on phase equilibrium at the ablating surface and on the simplified film-coefficient approach for unity Lewis-Semenov number. Limited test data from the Avco Model 500 arc are compared with the predictions based on equilibrium thermochemistry, and discrepancies are discussed and explained. The thermochemical models are used to compare the ablative performance of these materials in a typical high-performance nosetip environment, and the most attractive materials, from this standpoint, are identified.

Nomenclature

c_p = specific heat
C = constant defined by Eq. (35)
D = diameter of test specimen
f = fraction of silicon vaporized
ΔF_I = standard molal free energy of formation of specie I at surface temperature
h = heat-transfer coefficient based on enthalpy driving force
h_o = heat-transfer coefficient in the absence of mass transfer
H_e = recovery enthalpy, BTU/lbm
H_s = enthalpy of heat-shield material at surface temperature, BTU/lbm
H_w = enthalpy of undissociated freestream gas at wall temperature
H_I = enthalpy of specie I at surface temperature
H_∞ = enthalpy of heat-shield material at its initial temperature
ΔH_c = energy absorbed by chemical reactions and phase changes at the ablating surface per unit mass of heat shield, BTU/lbm
ΔH_I = molal heat of formation of specie I at surface temperature
k = thermal conductivity
k_o = thermal conductivity at surface temperature, BTU/hr ft R
K_i = equilibrium constant for reaction Ri
K_I = mass fraction of specie I at the wall
$\tilde{K}_{Ie}$ = mass fraction of I atoms in freestream
$\dot{m}$ = mass removal rate, lbm/sec ft^2
$\dot{m}_I$ = production rate of specie I at the wall
M_n = molecular weight of nontransferred gas
M_I = formula weight of I
n = tantalum-carbon atom ratio in condensed-phase reaction product; silicon-carbon atom ratio in equilibrium liquid phase
n_p = value of n at peritectic temperature
$\bar{n}$ = silicon-carbon atom ratio in condensed-phase reaction product
p = exponent defined by Eq. (9)
P = surface pressure, atm
P_I = partial pressure of specie I at the wall
$(P_I)_i$ = partial pressure of specie I at the wall based on reaction Ri equilibrium
$(P_{SiO})_D$ = partial pressure of SiO at the wall based on complete diffusion-limited oxidation
$\dot{q}$ = heat-transfer rate to cold inert wall, BTU/sec ft^2
$\dot{q}_c$ = chemical energy flux, $-\dot{m}\Delta H_c$, BTU/sec ft^2
$\dot{q}_{cw}$ = heat-transfer rate to water-cooled calorimeter, BTU/sec ft^2
$\dot{q}_d$ = $k_o T/D$
$\dot{q}_h$ = heat-transfer rate defined by Eq. (2)
$\dot{q}_k$ = conducted flux in heat-shield material at ablating surface
$\dot{q}_{ko}$ = energy flux required to bring heat-shield material to surface temperature, BTU/sec ft^2
$\dot{q}_r$ = energy flux radiated from ablating surface, BTU/sec ft^2
$\dot{q}_{rs}$ = radiation from lateral surface of test specimen per unit cross-sectional area, BTU/sec ft^2
$\dot{q}_s$ = net heat-transfer rate to heat-shield material at ablating surface, $\dot{q}_h + \dot{q}_c$
R = universal gas constant
$\dot{s}$ = surface recession rate, in./sec
t = temperature below surface of heat shield
T = surface temperature, deg R
T_m = melting point of TaC
T_p = peritectic decomposition temperature of Ta_2C or SiC R
T_B = brightness temperature, R
x = distance from ablating surface into heat shield
y = carbon-oxygen atom ratio in freestream
z = nitrogen-oxygen atom ratio in freestream
γ = fraction of condensed-phase silicon oxidized to SiO_2
ε = surface total emissivity
ε_λ = spectral emissivity at wavelength, λ
η = blowing coefficient based on total mass-removal rate
η_I = blowing coefficient of specie I
λ = wavelength, μ
ρ = heat-shield density, lbm/ft^3
σ = Stefan-Boltzmann constant

Presented as Paper 74-517 at the AIAA 7th Fluid and Plasma Dynamics Conference, Palo Alto, California, June 17–19, 1974; submitted July 17, 1974; revision received November 1, 1974.
Index categories: Material Ablation; Thermochemistry and Chemical Kinetics.
* Senior Consulting Scientist.

Introduction

THE need for a re-entry vehicle nosetip combining good resistance to mechanical erosion in clouds and rain with acceptable ablation performance has aroused renewed interest in various metallic and ceramic heat-shield materials and in techniques for predicting their thermochemical ablative performance in high-enthalpy air. In this paper, prediction models are derived for a number of such materials, based on the following principal simplifying assumptions.

1) All gaseous and condensed-phase reaction products are in equilibrium with the solid heat-shield material at the ablating surface. This implies that condensed-phase reaction products are removed immediately or can sustain only very thin surface layers.

2) The film-coefficient model developed by Lees,[1] based on an effective binary gas mixture with unity Lewis-Semenov number, is applicable. The validity of this assumption has been demonstrated for the carbon-air system,[2,3] but it has not been established for systems involving gaseous products with higher molecular masses.

Given these assumptions, the normalized ablation rate, $\dot{m}/h$, and heat of reaction, ΔH_c, of a single-component heat shield, at any specified surface temperature and pressure, can be determined as follows. Calculate the equilibrium composition of a mixture of heat-shield material and air, containing excess heat-shield material, at the specified temperature and pressure. Then the normalized ablation rate, $\dot{m}/h$, is simply the ratio of heat-shield mass lost, by phase change and/or chemical reaction, to mass of air entering the reaction. The heat of reaction is the net change in system energy (heat of formation of products less heat of formation of reactants) per unit mass of heat shield lost. Thus, by performing a series of chemical-equilibrium calculations at various combinations of temperature and pressure, the equilibrium thermochemical ablation performance of any material can be expressed as maps of $\dot{m}/h$ and ΔH_c vs surface temperature and pressure, and these maps can be used as inputs to generalized thermal-response computer programs.

This approach or its equivalent has been used by a number of investigators in their studies of carbon[3,4] and other materials.[5] An alternate approach, previously applied to carbon and carbon + inert systems,[6] specializes the equilibrium relationships to the specific material under study and combines them with the simplified boundary-layer transport equations to derive analytical expressions or simple algorithms for $\dot{m}/h$ and ΔH_c, eliminating the need for the pressure-temperature maps previously described. Where it is applicable, the latter approach has a number of significant advantages,[6] and it has been adopted here.

To simplify the resulting algorithms, the applicable temperature and pressure ranges are restricted, where necessary, to those normally encountered in low-altitude (< 100,000 ft) re-entry or in high-enthalpy plasma-arc facilities. Also, since test data have been obtained in the Avco Model 500 arc, in which the freestream contains significant quantities of carbon, the formulations include the effects of freestream carbon on the material response.

Basic Relations

The assumptions of equal binary diffusion coefficients and unity Lewis-Semenov number give rise to especially simple relationships describing the transport of matter and energy in chemically-reacting boundary layers on ablating bodies, in terms of conditions in the freestream and at the gas-solid interface. Stated most succinctly, conditions at the wall are the results of mixing injected material at surface temperature, at the rate $\dot{m}$, with freestream material at recovery enthalpy, at the rate h. Since both mass and energy are conserved in this process, the net heat-transfer rate to the wall is simply the resulting net enthalpy flux, i.e., the heat content of the reactants less that of the products at wall temperature. The enthalpy of the products depends on their chemical state, which can be estimated from phase-equilibrium relations. Thus the heat transfer at the ablating surface can be written as

$$\dot{q}_s = \dot{m}H_s + hH_e - (\dot{m}+h)\sum K_I H_I \tag{1}$$

which is essentially the form derived by Lees.[1] Let $\dot{q}_s = \dot{q}_h + \dot{q}_c$, where

$$\dot{q}_h = h(H_e - H_w) \tag{2}$$

$$\dot{q}_c = hH_w + \dot{m}H_s - (h+\dot{m})\sum K_I H_I \tag{3}$$

If H_w is defined as the enthalpy of the undissociated freestream gas at wall temperature (carbon as CO, oxygen as CO and O_2, nitrogen as N_2), then $\dot{q}_c$ is the heat-of-formation flux,

$$\dot{q}_c = -\sum \dot{m}_I \Delta H_I / M_I \tag{4}$$

where the summation is over all species, regardless of phase, at the ablating surface. The chemical energy per unit mass of heat shield, ΔH_c, is

$$\Delta H_c = -\dot{q}_c/\dot{m} = \sum (\dot{m}_I/\dot{m})(\Delta H_I/M_I) \tag{5}$$

Surface Energy Balance

The surface energy balance, including radiation and subsurface conduction, can now be written as

$$\dot{q}_h + \dot{q}_c = \dot{q}_k + \dot{q}_r \tag{6}$$

For one-dimensional steady-state ablation, $\dot{q}_k = \dot{q}_{ko} = \dot{m}(H_s - H_\infty)$. In plasma-arc testing of relatively high-conductivity materials, heat transfer from the lateral surface of the test specimen, by radiation and/or convection, may be important. In Appendix A, an approximate solution is obtained for the case of side-radiation only. For this case, $\dot{q}_k = \dot{q}_{ko} + \dot{q}_{rs}$, and

$$\dot{q}_{rs} = \left[\frac{\dot{q}_{ko}}{2} + \dot{q}_d \dot{q}_r \exp\left(-\frac{2\dot{q}_r}{7\dot{q}_d}\right)\right]^{1/2} - \frac{\dot{q}_{ko}}{2} \tag{7}$$

Except where otherwise indicated, calculations in this paper are based on thermochemical data in the most recent JANAF Tables.[7]

Blowing Correction

The effect of mass transfer on the heat/mass-transfer coefficient is conveniently expressed, for moderate blowing rates, by

$$h/h_o = 1/(1+\eta\dot{m}/h) \tag{8}$$

For foreign-gas injection, the blowing coefficient has been correlated, for both laminar and turbulent flows,[8,9] by expressions of the form

$$\eta_I = \eta_o(M_n/M_I)^p \tag{9}$$

where η_o is the blowing coefficient for like-gas injection, and M_I and M_n are the molecular weights of the transferred and nontransferred gases, respectively. Where two or more foreign gases are injected simultaneously, it seems reasonable to calculate an average blowing coefficient based on the relationship $\eta \sum \dot{m}_I = \sum \eta_I \dot{m}_I$, which, when combined with Eq. (9), gives

$$\eta\dot{m} = \eta_o \sum \dot{m}_I (M_n/M_I)^p \tag{10}$$

where the summation is over all gaseous species transferred to and from the wall. For a reacting boundary layer of the type considered here, this expression is still somewhat ambiguous, since the transferred species may change their relative concentrations and even their identities with distance from the wall. Also, since there may be net transport of oxygen from the freestream to the wall, the identities of the transferred and nontransferred gases may not always be obvious. To resolve these questions, three idealizations will be adopted here:

1) Oxygen is transported toward the wall at the rate required to form both gaseous and condensed-phase oxides. The oxygen is transported as O, O_2, and NO, in the proportions in which they are present at the wall. For the systems considered here, the O_2 concentration at the wall is negligible relative to either O or NO.

2) Gaseous reaction products are transported away from the wall at the rate at which they are produced at the ablating surface. The algebraic sum of this rate and the rate of oxygen transport, defined above, is equal to the net boundary-layer injection rate.

3) The nontransferred gas consists of O, O_2, NO, and N_2, in the proportions in which they are present at the wall. For the heat-shield systems considered here, the nontransferred gas is essentially pure N_2.

For the usual case in which oxygen is transported to the wall as O and NO at the rate $h\tilde{K}_{Oe}(1-y)$, while the nontransferred gas is N_2, Eq. (10) becomes

$$\eta\dot{m}/\eta_o = \sum \dot{m}_I (2M_N/M_I)^p - h\tilde{K}_{Oe}(1-y)(2M_N/M_O)^p \frac{P_O/P_{NO} + (M_O/M_{NO})^p}{P_O/P_{NO}+1} \tag{11}$$

where the summation now includes only product species. The equilibrium ratio P_{NO}/P_O is approximately

$$P_{NO}/P_O = 0.00137 P_{N_2}{}^{1/2} \exp(36{,}000/T) \tag{12}$$

Recommended values of the exponent p vary from 0.25 to 0.6,[8,9] depending on flow regime and other considerations. Calculations in this work are based on $p = 1/3$, $\eta_o = 2/3$.

Silicon Nitride

In the absence of oxygen, silicon nitride decomposes at high temperature to yield gaseous nitrogen and liquid silicon. The equilibrium nitrogen partial pressure varies from about one atm at 3900°R to about 200 atm at 5000°R, and surface temperatures for high-performance nosetips will generally fall in this range. In the presence of Si_3N_4, the equilibrium partial pressure of free oxygen is negligibly small, and so is that of NO. Since the vapor pressures of silicon and silica are also very small, N_2 and SiO are the only significant gaseous species at the wall (in air; when the freestream contains carbon, CO will be present as well). In

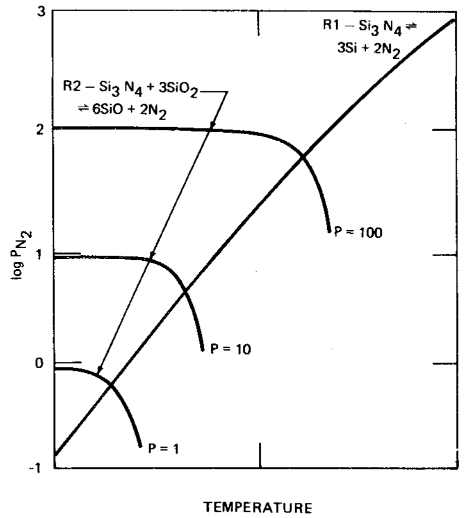

Fig. 1 Phase diagram for silicon-nitride ablation.

addition, P_{SiO} must be equal to or smaller than the equilibrium values determined from the following reactions, where it is assumed that the mutual solubilities of Si(l), SiO_2(l), and Si_3N_4(c) can be neglected.

$$Si_3N_4(c) \rightleftharpoons 3Si(l) + 2N_2(g) \tag{R1}$$

$$Si_3N_4(c) + 3SiO_2(l) \rightleftharpoons 6SiO(g) + 2N_2(g) \tag{R2}$$

A few calculations in the temperature and pressure ranges of interest suffice to establish the form of the resulting phase diagram, as shown in Fig. 1. Reaction R1 gives a single curve in these coordinates; reaction R2 gives a series of curves, with pressure as the parameter. In the region above the curves, the reaction products are N_2 and SiO, and the only condensed phase is Si_3N_4. On the curves for reaction R2, SiO_2 is an additional reaction product, and reaction R2 equilibrium is satisfied. On the reaction R1 equilibrium curves, the additional reaction product is liquid silicon. In the region below curves R2, reaction R2 proceeds to the left, increasing the nitrogen partial pressure until R2 equilibrium is restored. Below curve R1, silicon nitride decomposes, again increasing N_2 partial pressure to satisfy equilibrium. Both equilibria are satisfied at the intersections, where all three condensed phases, Si_3N_4, Si, and SiO_2, coexist.

The overall heat-shield/freestream reaction can be described by the balanced chemical equation

$$\overbrace{\tfrac{1}{3}Si_3N_4}^{H/S} + \overbrace{\frac{f+2(1-f)\gamma}{1-y}(O+yC+zN)}^{\text{freestream}} \rightarrow$$

$$fSiO + (1-f)(1-\gamma)Si + (1-f)\gamma SiO_2 + \left[\frac{2}{3} + \frac{f+2(1-f)\gamma}{1-y}\frac{z}{2}\right]N_2$$

where f is the fraction of silicon vaporized (as SiO) and γ is the fraction of condensed-phase silicon oxidized to SiO_2. The mol fraction of SiO at the wall is

$$P_{SiO}/P = \frac{f}{\frac{2}{3}+f+[f+2(1-f)\gamma]\dfrac{y+z/2}{1-y}} \tag{13}$$

where the numerator is the coefficient of SiO in the chemical equation, and the denominator is the sum of the coefficients of SiO, N_2, and CO. Similarly, for N_2,

$$P_{N_2}/P = \frac{\frac{2}{3}+[f+2(1-f)\gamma]\dfrac{z/2}{1-y}}{\frac{2}{3}+f+[f+2(1-f)\gamma]\dfrac{y+z/2}{1-y}} \tag{14}$$

Equations (13) and (14) can be combined, eliminating f, to give

$$P_{SiO}/P = \frac{\frac{2}{3}(1-y)+\gamma z-[\frac{2}{3}(1-y)+\gamma(2y+z)]P_{N_2}/P}{\frac{2}{3}+\gamma(z-4y/3)} \tag{15}$$

In the region of Fig. 1 above the equilibrium curves, where $f = 1.0$, Eq. (13) becomes

$$(P_{SiO})_D = \frac{P}{\dfrac{2}{3}+\dfrac{1+z/2}{1-y}} \tag{16}$$

Based on reaction R1 equilibrium ($\gamma = 0$),

$$(P_{N_2})_1 = \exp\left(\frac{\Delta F_{Si_3N_4}}{2RT}\right) \tag{17}$$

and, substituting this in Eq. (15),

$$(P_{SiO})_1 = (1-y)\left[P - \exp\left(\frac{\Delta F_{Si_3N_4}}{2RT}\right)\right] \tag{18}$$

Based on reaction R2 equilibrium ($\gamma = 1.0$),

$$P_{N_2}P_{SiO}{}^3 = K_2 = \exp\left(\frac{1.5\Delta F_{SiO_2}+0.5\Delta F_{Si_3N_4}-3\Delta F_{SiO}}{RT}\right) \tag{19}$$

Combining this with Eq. (15) gives

$$(P_{SiO})_2/P = \left[\frac{(1+3z/2+2y)K_2/P^4}{1+3z/2-y-(1+3z/2-2y)(P_{SiO})_2/P}\right]^{1/3} \tag{20}$$

which is readily solved for $P_{SiO})_2$ by iteration. Since only values equal to or less than equilibrium are permitted, the partial pressure of SiO must be the smallest of the three possible values,

$$P_{SiO} = \min\,[(P_{SiO})_D, (P_{SiO})_1, (P_{SiO})_2] \tag{21}$$

Equation (13) can be solved for f,

$$f = \frac{2(1-y)/3+\gamma(z+2y)}{(1-y)P/P_{SiO}+\gamma(z+2y)-1-z/2} \tag{22}$$

The normalized mass recession rate is the ratio of heat-shield mass to freestream mass entering the reaction,

$$\dot{m}/h = \frac{(1-y)\tilde{K}_{Oe}}{f+2(1-f)\gamma}\frac{M_{Si_3N_4}}{3M_O} \tag{23}$$

Equation (11) now becomes

$$\eta/\eta_o = \frac{2M_N}{M_{Si_3N_4}}\left\{2+3f\left(\frac{M_{SiO}}{2M_N}\right)^{1-p} - 3[f+2(1-f)\gamma]\left(\frac{M_O}{2M_N}\right)^{1-p}\frac{P_O/P_{NO}+(M_O/M_{NO})^p}{P_O/P_{NO}+1}\right\} \tag{24}$$

or, with $p = 1/3$,

$$\eta/\eta_o = 0.4\left\{1+2.03f-1.03[f+2(1-f)\gamma]\frac{1+0.81P_{NO}/P_O}{1+P_{NO}/P_O}\right\} \tag{25}$$

The reaction energy, ΔH_c, is, from Eq. (5),

$$\Delta H_c = [-\Delta H_{Si_3N_4}+3f\Delta H_{SiO}+3(1-f)\gamma\,\Delta H_{SiO_2}]/M_{Si_3N_4} \tag{26}$$

Given the freestream conditions (composition and enthalpy), the nonblowing heat-transfer rate, and the surface pressure, the ablation rate can be calculated as follows:

1) Select a trial surface temperature and calculate the equilibrium constant K_2 from Eq. (19).

2) Calculate $(P_{SiO})_D$, $(P_{SiO})_1$, and $(P_{SiO})_2$ from Eqs. (16), (18), and (20). Select P_{SiO} from Eq. (21). If $P_{SiO} = (P_{SiO})_2$, $\gamma = 1.0$, otherwise $\gamma = 0$.

3) Calculate f from Eq. (22), $\dot{m}/h$ from Eq. (23), P_{N_2} from Eq. (14), η from Eqs. (12) and (25), h from Eq. (8), and ΔH_c from Eq. (26).

4) Check the surface energy balance, Eq. (6).

5) If necessary, select a new trial surface temperature and start over. If, over a very narrow temperature range, the solution changes from R2 equilibrium with positive energy imbalance ($\dot{q}_h+\dot{q}_c > \dot{q}_r+\dot{q}_k$) to R1 equilibrium with negative imbalance, the correct solution will be at the intersection of the equilibrium curves ($0 < \gamma < 1$). The computation then proceeds as follows:

6) Select T such that $(P_{SiO})_2 = (P_{SiO})_1$. Assume a value of γ. Repeat Steps 3 and 4 above, adjusting γ as required until the energy equation is satisfied.

Tantalum Carbide

The thermodynamics of tantalum-carbide ablation in air are comparatively simple, since the only significant gaseous reaction product at typical re-entry surface temperatures is carbon monoxide. The stable condensed-phase reaction product is ditantalum carbide, Ta_2C, up to its peritectic decomposition temperature, about 6790°R.[10,12] As its peritectic temperature, Ta_2C decomposes to yield solid tantalum carbide and a stable liquid phase. According to the carbon-tantalum phase diagram adopted by Hansen,[11] the composition of the liquid phase can be expressed as Ta_nC, where n varies nearly linearly with temperature from about 2.6 at the Ta_2C peritectic to 1.0 at the melting point of tantalum carbide. The overall oxidation reaction, then, can be written as

$$\mathrm{TaC} + \frac{n-1}{2n}\mathrm{O}_2 \rightarrow \frac{1}{n}\mathrm{Ta}_n\mathrm{C} + \frac{n-1}{n}\mathrm{CO}$$

where

$$n = 2 \qquad [T < T_p]$$
$$n = 1 + 1.6(T_m - T)/(T_m - T_p) \qquad [T > T_p]$$
$$2 < n < 2.6 \qquad [T = T_p]$$

The normalized mass recession rate is

$$\dot{m}/h = \frac{(1-y)n}{n-1}\tilde{K}_{\mathrm{O}e} M_{\mathrm{TaC}}/M_{\mathrm{O}} \tag{27}$$

Combining Eqs. (11) and (27), the blowing correction is evaluated from

$$\frac{\eta}{\eta_o}\frac{\dot{m}}{h} = (1-y)\tilde{K}_{\mathrm{O}e}\frac{2M_{\mathrm{N}}}{M_{\mathrm{O}}}\left[\left(\frac{M_{\mathrm{CO}}}{2M_{\mathrm{N}}}\right)^{1-p} - \left(\frac{M_{\mathrm{O}}}{2M_{\mathrm{N}}}\right)^{1-p}\frac{P_{\mathrm{O}}/P_{\mathrm{NO}} + (M_{\mathrm{O}}/M_{\mathrm{NO}})^p}{P_{\mathrm{O}}/P_{\mathrm{NO}} + 1}\right] \tag{28}$$

where $P_{\mathrm{NO}}/P_{\mathrm{O}}$ is calculated from Eq. (12) and P_{N_2} from

$$P_{\mathrm{N}_2} = P/(1 + 2/z) \tag{29}$$

Setting $p = 1/3$,

$$\frac{\eta}{\eta_o}\frac{\dot{m}}{h} = \tilde{K}_{\mathrm{O}e}(1-y)\left(1.75 - 1.21\frac{1 + 0.81P_{\mathrm{NO}}/P_{\mathrm{O}}}{1 + P_{\mathrm{NO}}/P_{\mathrm{O}}}\right) \tag{30}$$

Below the Ta_2C peritectic temperature, the chemical reaction energy is

$$\Delta H_c = (-\Delta H_{\mathrm{TaC}} + 0.5\Delta H_{\mathrm{CO}} + 0.5\Delta H_{\mathrm{Ta_2O}})/M_{\mathrm{TaC}} \tag{31}$$

Enthalpy data are not available for the stable liquid phase at higher temperatures. Assuming that $Ta_nC(l)$ has the same enthalpy as a mechanical mixture of liquid tantalum and liquid tantalum carbide of the same overall composition, the chemical reaction energy in this temperature range is

$$\Delta H_c = \frac{-\Delta H_{\mathrm{TaC}} + [(n-1)\Delta H_{\mathrm{CO}} + \Delta H_{\mathrm{TaC(l)}}]/n}{M_{\mathrm{TaC}}} \tag{32}$$

When $T = T_p$, ΔH_c takes on whatever intermediate value will satisfy the energy balance, Eq. (6),

$$\Delta H_c = \frac{-n\,\Delta H_{\mathrm{TaC}} + (n-1)\,\Delta H_{\mathrm{CO}} + [(13-5n)\,\Delta H_{\mathrm{Ta_2C}} + 5(n-2)\,\Delta H_{\mathrm{TaC(l)}}]/3}{nM_{\mathrm{TaC}}} \tag{33}$$

where $2 < n < 2.6$. For Ta_2C, the thermochemical data compiled by Schick, et al[10] appear to be the best available.

Silicon Carbide

At a temperature somewhat higher than 5000°R, pure silicon carbide undergoes peritectic decomposition, yielding an equilibrium mixture of graphite and a liquid phase of fixed but uncertain composition, Si_nC. Both the peritectic temperature and the silicon-carbon ratio, n, are rather ill-defined, with reported values ranging from 5000 to 5600°R and from 2.7 to 4.3, respectively.[12] When oxidized in air at lower temperatures, only the liquid phase will be present (along with the gaseous reaction products), with higher, but equally uncertain values of n. In view of these uncertainties, a highly sophisticated model of the ablation process does not appear to be warranted. Therefore, the formulation presented here will be strictly applicable only at, or slightly below, the peritectic decomposition temperature. Currently available data suggest that steady-state surface temperature will always be close to T_p in both the Model 500 arc and the more severe nosetip re-entry environment.

At this temperature level, the significant gaseous ablation products are Si, Si_2, SiC_2, Si_2C, SiO, and CO. The condensed-phase species participating in the surface equilibrium are SiC, liquid Si_nC, and, at the peritectic temperature only, solid carbon. The partial free energy of formation of silicon in the liquid phase is, for an ideal solution,

$$\Delta F_{\mathrm{Si(l)}} = RT\ln\frac{n}{n+1} \tag{34}$$

Assuming that the partial free energy of mixing is independent of temperature and proportional to the square of the carbon mol fraction,

$$\Delta F_{\mathrm{Si(l)}} = RT\ln\frac{n}{n+1} + \mathrm{C}/(n+1)^2 \tag{35}$$

At the peritectic temperature, $\Delta F_{\mathrm{Si(l)}} = \Delta F_{\mathrm{SiC}}$, and the constant C can be evaluated,

$$\mathrm{C} = \left[(\Delta F_{\mathrm{SiC}})_{T_p} - RT_p\ln\frac{n_p}{n_p+1}\right](n_p+1)^2 \tag{36}$$

The partial pressures of the gaseous products at the wall can be formulated by consideration of the mutually independent chemical reactions,

$$\mathrm{Si(l)} \rightleftharpoons \mathrm{Si(g)} \tag{R3}$$
$$2\mathrm{Si(l)} \rightleftharpoons \mathrm{Si_2(g)} \tag{R4}$$
$$2\mathrm{SiC(c)} \rightleftharpoons \mathrm{Si(l)} + \mathrm{SiC_2(g)} \tag{R5}$$
$$\mathrm{SiC(c)} + \mathrm{Si(l)} \rightleftharpoons \mathrm{Si_2C(g)} \tag{R6}$$
$$2\mathrm{Si(l)} + \mathrm{CO(g)} \rightleftharpoons \mathrm{SiC(c)} + \mathrm{SiO(g)} \tag{R7}$$

for which the equilibrium relations are, respectively,

$$P_{\mathrm{Si}} = \exp\left(\frac{\Delta F_{\mathrm{Si(l)}} - \Delta F_{\mathrm{Si}}}{RT}\right) \tag{37}$$

$$P_{\mathrm{Si_2}} = \exp\left(\frac{2\Delta F_{\mathrm{Si(l)}} - \Delta F_{\mathrm{Si_2}}}{RT}\right) \tag{38}$$

$$P_{\mathrm{SiC_2}} = \exp\left(\frac{2\,\Delta F_{\mathrm{SiC}} - \Delta F_{\mathrm{Si(l)}} - \Delta F_{\mathrm{SiC_2}}}{RT}\right) \tag{39}$$

$$P_{\mathrm{Si_2C}} = \exp\left(\frac{\Delta F_{\mathrm{SiC}} + \Delta F_{\mathrm{Si(l)}} - \Delta F_{\mathrm{Si_2C}}}{RT}\right) \tag{40}$$

$$P_{\mathrm{SiO}}/P_{\mathrm{CO}} = K_7 = \exp\left(\frac{2\,\Delta F_{\mathrm{Si(l)}} - \Delta F_{\mathrm{SiC}} + \Delta F_{\mathrm{CO}} - \Delta F_{\mathrm{SiO}}}{RT}\right) \tag{41}$$

The nitrogen-oxygen ratio at the wall is equal to that in the freestream,

$$P_{\mathrm{N}_2}/(P_{\mathrm{SiO}} + P_{\mathrm{CO}}) = z/2 \tag{42}$$

and the static pressure is the sum of the partial pressures,

$$P = \sum P_I \tag{43}$$

The last three equations are readily solved for P_{N_2}, P_{SiO}, and P_{CO},

$$P_{\mathrm{N}_2} = \frac{P - P_{\mathrm{Si}} - P_{\mathrm{Si_2}} - P_{\mathrm{SiC_2}} - P_{\mathrm{Si_2C}}}{1 + 2/z} \tag{44}$$

$$P_{\mathrm{CO}} = \frac{2P_{\mathrm{N}_2}}{z(1+K_7)} \tag{45}$$

$$P_{\mathrm{SiO}} = K_7 P_{\mathrm{CO}} \tag{46}$$

The normalized production rate of any reaction product, $\dot{m}_I/h$, is equal to its mass concentration at the wall relative to that of air (however transformed chemically),

$$\dot{m}_I/h = \frac{P_I M_I \tilde{K}_{\mathrm{O}e}/M_{\mathrm{O}}}{P_{\mathrm{CO}} + P_{\mathrm{SiO}}}\,[I = \mathrm{Si, Si_2, SiC_2, Si_2C, SiO}] \tag{47}$$

Table 1 Data for ceramic composites in model 500 arc

Material	Run	Reinforcement	$H_e{}^a$	$\tilde{K}_{Ce}$	$\dot{q}_{cw}$	$T_B(\lambda)$	$\dot{s}_{\exp}$	$\dot{q}_r$	ρ	k_o
Si_3N_4	1601	2-D moly wires	9270	0.042	990	4260 (0.65)	0.0082	110	190	4.0
	1609	2-D BN filaments	8260	0.029	1010	4040 (0.8) 4300 (0.65)	0.0079	98	190	4.0
TaC	1603	W honeycomb	8630	0.033	990	5450 (0.65)	0.0068	162	810	26
	1611	3-D carbon rods	9210	0.040	1010	5000 (0.8) 5250 (0.65)	0.0055	170	810	26
SiC	1602	2-D carbon rods	9540	0.047	1020		0.0062	141	175	3.0
	1604	2-D carbon rods	8840	0.035	960		0.0062	131	175	3.0
	1608	2-D carbon rods	8730	0.034	1020	4700 (0.8) 5000 (0.65)	0.0043	150	190	3.0
	1610	3-D carbon rods	9160	0.040	1000	4730 (0.8) 4800 (0.65)	0.0044	140	190	3.0

[a] Relative to elements at absolute zero.

For CO, however, allowance must be made for the presence of carbon in the freestream,

$$\dot{m}_{CO}/h = \left(\frac{P_{CO}}{P_{CO}+P_{SiO}} - y\right)\tilde{K}_{Oe} M_{CO}/M_O \tag{48}$$

For $p = 1/3$, Eq. (11) becomes

$$\frac{\eta}{\eta_o}\frac{\dot{m}}{h} = \dot{m}_{CO}/h + \dot{m}_{Si}/h + 0.79\dot{m}_{Si_2}/h + 0.81\dot{m}_{SiC_2}/h + 0.74\dot{m}_{Si_2C}/h + 0.86\dot{m}_{SiO}/h - 1.21\tilde{K}_{Oe}(1-y)\frac{1+0.81P_{NO}/P_O}{1+P_{NO}/P_O} \tag{49}$$

where P_{NO}/P_O can be evaluated from Eq. (12). The chemical energy flux, $\dot{q}_c$, can be calculated from Eq. (4). Neglecting the heat of solution of carbon in liquid silicon,

$$\dot{q}_c = \dot{m}\,\Delta H_{SiC}/M_{SiC} - \sum \dot{m}_I\,\Delta H_I/M_I \tag{50}$$

where the summation is over all gaseous ablation products. The recession rate, $\dot{m}$, is determined by solving the energy balance, Eq. (6).

The ratio of silicon atoms to carbon atoms in the condensed-phase product is

$$\bar{n} = \frac{\dfrac{\dot{m}}{M_{SiC}} - \dfrac{\dot{m}_{Si}+\dot{m}_{Si_2}}{M_{Si}} - \dfrac{\dot{m}_{SiC_2}}{M_{SiC_2}} - \dfrac{2\dot{m}_{Si_2C}}{M_{Si_2C}} - \dfrac{\dot{m}_{SiO}}{M_{SiO}}}{\dfrac{\dot{m}}{M_{SiC}} - \dfrac{2\dot{m}_{SiC_2}}{M_{SiC_2}} - \dfrac{\dot{m}_{Si_2C}}{M_{Si_2C}} - \dfrac{\dot{m}_{CO}}{M_{CO}}} \tag{51}$$

If the surface temperature is equal to the peritectic temperature, $\bar{n}$ must be equal to or less than n, the value for the equilibrium liquid phase. For lower temperatures, $\bar{n} = n$. The calculations can proceed as follows:

1) Assume $T = T_p$.
2) Calculate partial pressures of all gaseous species and all $\dot{m}_I/h$. Correct h_o for blowing, and calculate all $\dot{m}_I$.
3) Solve surface energy balance for $\dot{m}$ and calculate $\bar{n}$.
4) If $\bar{n} \leq n_p$, solution is complete. If $\bar{n} > n_p$, select a lower surface temperature.
5) Repeat Steps 2 and 3, varying surface temperature, until $\bar{n} \cong n(T)$.

Elliott[12] presents two possible phase diagrams for the carbon-silicon system. One of these, with a peritectic temperature of about 5060°R and a liquid-phase silicon-carbon ratio of 2.7, leads to ablation-rate predictions substantially greater than the measured values. The other, with $T_p = 5585 \pm 72$°R and $n_p = 4.3$, is consistent with recession measurements. Calculations in this paper are based on $T_p = 5544$°R. Below the peritectic temperature, the liquid-phase composition is approximately

$$n = 4.3\exp\left[(T_p - T)/210\right] \tag{52}$$

Experimental Data

The principal source of experimental data for ceramic materials is a recent series of laminar-splash tests in the Avco Model 500 Arc.[13] This facility produces a high-enthalpy subsonic jet which exhausts directly into the laboratory from a 0.5-in.-diam exit nozzle. The jet enthalpy is estimated from a steady-state energy balance on the arc generator. Oxidation of the carbon cathode injects a significant quantity of carbon into the jet, reducing the available oxygen content as well as the effective enthalpy. The actual carbon content at the centerline of the jet is estimated from direct measurements under arc conditions similar to those used here. All specimens were 3/4-in.-diam flat-faced cylinders of reinforced ceramic material, mounted in an insulated brass holder and positioned one inch downstream of the nozzle exit plane. The heating rates were experimentally measured by a calibrated flat-faced water-cooled calorimeter prior to each test run. Surface brightness temperatures and total radiation were recorded from Thermodot (0.8 μ) and IDL (0.65 μ) pyrometers and an Eppley thermopile. Surface-recession data were obtained from silhouette photographs, using a 35-mm profile camera at one frame per second. In all cases, recession was quite uniform over the heated face. Most runs were about 30 sec long, and the recession rate was essentially constant for at least the last 10 sec of each run.

Since the jet is smaller in diameter than the test specimens, convective heating on the lateral surfaces is very small. Side radiation may be significant, however, especially when the specimen thermal conductivity is large, and the surface energy balance is modified accordingly, using the expression for side-radiation flux derived in Appendix A.

Test conditions and experimental data are shown in Table 1, along with the estimated physical properties used for data reduction. Stagnation pressure was 1.13 atm for all runs. A variety of reinforcements were used in fabricating the test specimens; ablation-rate predictions, however, are based on pure heat-shield material in each case. The calculations, based on the models presented here, are summarized in Table 2, which gives the calculated blowing reduction, surface temperature, and surface energy-balance terms, along with the ratio of calculated to experimental recession and the surface emissivities. The latter are calculated from the predicted surface temperature and the experimental radiometric data.

For silicon nitride, the predicted surface temperatures are well below the measured brightness temperatures, and the derived total emissivities are close to one, suggesting that the predicted temperatures are much too low. In spite of this, the recession-rate predictions are quite good. The most likely reason for the discrepancy in temperature is the existence of large nonequilibrium effects at the ablating surface. For example, the

Table 2 Model 500 Arc data reduction

Material	Run	$T(R)$	h/h_o	$\dot{q}_c$	$\dot{q}_{ko}$	$\dot{q}_{rs}$	$\dot{s}/\dot{s}_{\exp}$	ε	$\varepsilon_{0.65}$	$\varepsilon_{0.8}$
Si_3N_4	1601	3850	0.60	−269	103	26	0.87	1.05	2.7	
	1609	3850	0.60	−276	114	26	1.01	0.93	2.9	1.5
TaC	1603	7080	0.93	−64	220	237	0.89	0.14	0.20	
	1611	7130	0.93	−61	212	261	1.06	0.14	0.14	0.15
SiC	1602	5540	0.71	−259	143	31	1.06	0.31		
	1604	5540	0.71	−242	125	30	0.91	0.29		
	1608	5540	0.71	−251	123	37	1.18	0.33	0.46	0.35
	1610	5540	0.71	−250	130	36	1.24	0.31	0.33	0.37

liquid-silicon layer may be thick enough to give a surface temperature well in excess of the solid-liquid interface temperature; or the silicon nitride may decompose too slowly at near-equilibrium conditions, thus requiring substantial superheat to attain the rates involved in these tests. Additional data, over a range of test environments, will be required to resolve these uncertainties. Meanwhile, the success of the model in predicting recession rates suggests that it can be used for this purpose, with reasonable confidence, even at conditions somewhat removed from those in the Model 500 facility.

The recession predictions of the tantalum-carbide model are also quite good, with less than 10% disagreement for both tests. The derived total and spectral emissivities seem low, but may not be unreasonable for a thin layer of liquid (with the approximate composition Ta_2C in both cases) over solid TaC. In any case, there are no emissivity data available for comparison, and the consistency of these results is encouraging. The importance of side radiation in these tests is noteworthy; well over one third of the net convective heating is radiated from the lateral surface of the specimen, more than is required to heat the material to surface temperature.

The silicon-carbide results are also quite good, although the predicted recession rates are slightly high, on the average. Agreement between predicted and measured recession rates can be improved by assuming a slightly larger value for the SiC peritectic decomposition temperature. For example, increasing T_p only nine degrees changes $\dot{s}/\dot{s}_{\exp}$ for Run 1610 from 1.24 to 1.16, with comparable changes for the other runs. This sensitivity to temperature arises largely from its effect on the vaporization rates of Si, SiC_2, and Si_2C. Thus, at higher pressures, where these species are less important, the ablation rate is much less sensitive to peritectic temperature.

Re-Entry Performance

Based on the models derived here, the thermochemical ablative response of these materials has been calculated for a typical high-performance re-entry nosetip environment, and the results are summarized in Table 3. Also shown are comparable data for tungsten, a leading metallic candidate material. All calculations are based on one-dimensional steady-state response, with no allowances for heating enhancement by roughness or other special effects. The assumed densities, shown in the table, are 95% of theoretical for the ceramic materials, and 100% for tungsten. Also shown in the table are the blowing correction factor, h/h_o, the surface temperature, the mass-loss and surface-recession rates, $\dot{m}$ and $\dot{s}$, and the energies "absorbed" per unit mass of heat shield by blowing, $\eta(H_e - H_w)$, by chemical reactions and phase changes at the heated surface, ΔH_c, by heating of the heat-shield material to surface temperature, $H_s - H_\infty$, and by radiation, $\dot{q}_r/\dot{m}$.

Table 3 Re-entry performance[a]

Material	Si_3N_4	TaC	SiC	W
ρ	190	850	190	1200
h/h_o	0.58	0.90	0.89	0.88
T	4730	7250	5540	6620
$\dot{m}$	1.13	7.06	2.25	17.1
$\dot{s}$	0.071	0.100	0.142	0.171
$\eta(H_e - H_w)$	2600	80	310	43
ΔH_c	2100	150	970	20
$H_s - H_\infty$	1200	560	1500	280
$\dot{q}_r/\dot{m}$	210	26	62	16

[a] $P = 100$ $H_e = 8000$ $\dot{q} = 8000.$

Silicon nitride is clearly the best performer in this environment and tungsten the poorest, with silicon carbide and tantalum carbide somewhere between them, depending on whether mass loss or surface recession is the more important variable. The superiority of silicon nitride is largely the result of its large blowing correction, although surface reactions also absorb energy quite effectively. Tungsten is the poorest energy absorber, per unit mass, by every mechanism. It is interesting, also, to note the reversal in relative ranking among the ceramics, based on surface recession, in high-pressure and low-pressure environments. In the Model 500 Arc (Table 1), silicon carbide had the lowest $\dot{s}$ and silicon nitride the highest, under comparable conditions. At high pressures, the silicon-carbide surface temperature is still limited to T_p, but vaporization of Si, Si_2, SiC_2, and Si_2C is suppressed, decreasing specific energy absorption both by blowing and surface reactions. Silicon nitride has no such upper limit on surface temperature, and the equilibrium partial pressures of its gaseous ablation products tend to increase proportionately at high surface pressures.

Appendix A: Effect of Side Radiation on Steady-State Energy Balance

Consider a circular-cylindrical ablating body, uniformly heated on one end ($x = 0$) and subject to radiative cooling from both its heated and lateral surfaces. A steady-state energy balance over a differential element leads to the equation

$$\frac{d}{dx} k \frac{dt}{dx} + \dot{m} c_p \frac{dt}{dx} = \frac{4}{D} \varepsilon\sigma t^4 \left(1 - \frac{\varepsilon\sigma t^3 D}{8k_o}\right)^4$$

where the factor in parentheses is an approximate correction to account for radial temperature gradients. An approximate integral solution to the equation is readily obtained, based on the assumed temperature distribution $t = Te^{-x/\delta}$. Integrating between the limits $x = 0$ and $x = \infty$, the differential equation becomes

$$\frac{k_o T}{\delta} - \dot{m}(H_s - H_\infty) = \frac{4\varepsilon\sigma}{D} \int_0^\infty t^4 \left(1 - \frac{\varepsilon\sigma t^3 D}{8k_o}\right)^4 dx$$

Completing the integration,

$$\frac{k_o T}{\delta} - \dot{m}(H_s - H_\infty) = \varepsilon\sigma T^4 \frac{\delta}{D}\left(1 - \frac{2\xi}{7} + \frac{3\xi^2}{80} - \frac{\xi^3}{416} + \frac{\xi^4}{16384}\right)$$

where $\xi = \varepsilon\sigma T^3 D/k_o$. For ξ less than about six, this is closely approximated by

$$\frac{k_o T}{\delta} - \dot{m}(H_s - H_\infty) = \varepsilon\sigma T^4 \frac{\delta}{D} e^{-2\xi/7}$$

where the right-hand side is the total side radiation flux, $\dot{q}_{rs}$. Solving for δ and substituting the result in the right-hand side gives

$$\dot{q}_{rs} = \left[\left(\frac{\dot{q}_{ko}}{2}\right)^2 + \dot{q}_d \dot{q}_r \exp\left(-\frac{2\dot{q}_r}{7\dot{q}_d}\right)\right]^{1/2} - \frac{\dot{q}_{ko}}{2}$$

where $\dot{q}_{ko} = \dot{m}(H_s - H_\infty)$, $\dot{q}_d = k_o T/D$, and $\dot{q}_r = \varepsilon\sigma T^4$.

References

[1] Lees, L., "Convective Heat Transfer with Mass Addition and Chemical Reactions," *Recent Advances in Heat and Mass Transfer*, edited by J. P. Hartnett, McGraw-Hill, New York, 1961.

[2] Hearne, L. F., Gallagher, L. W., and Woodruff, L. W., "Surface Oxidation with Streamwise Variation of Wall Reactivity," *AIAA Progress in Astronautics and Aeronautics: Thermal Design Principles of Spacecraft and Entry Bodies*, Vol. 21, edited by J. T. Bevans, Academic Press, New York, 1969, pp. 225–248.

[3] Dolton, T. A., Maurer, R. E., and Goldstein, H. E., "Thermodynamic Performance of Carbon in Hyperthermal Environments," *AIAA Progress in Astronautics and Aeronautics: Thermal Design Principles of Spacecraft and Entry Bodies*, edited by J. T. Bevans, Academic Press, New York, 1969, pp. 169–201.

[4] Kratsch, K. M., Martinez, M. R., Clayton, F. I., Greene, R. B., and Wuerer, J. E., "Graphite Ablation in High-Pressure Environments," AIAA Paper 68-1153, Williamsburg, Va., Dec. 1968.

[5] Moody, H. L., Sherman, M. M., Dunn, S. S., and Haddock, R. L., "The Development and Application of a Tungsten Ablation Model for Reentry Environments," PDA TR 1013-00-05, Jan. 1974, Prototype Development Associates, Inc., Costa Mesa, Calif.

[6] Ziering, M. B. and DiCristina, V., "Thermomechanical Erosion of Ablative Plastic Composites," AIAA Paper 72-299, San Antonio, Texas, April 1972.

[7] *JANAF Thermochemical Tables*, Dow Chemical Company, Midland, Mich., incl. Supplement No. 41, June 1974.

[8] Hartnett, J. P., "Mass Transfer Cooling," *Handbook of Heat Transfer*, edited by W. M. Rohsenow and J. P. Hartnett, McGraw-Hill, New York, 1973.

[9] Rubesin, M. W. and Inouye, M., "Forced Convection, External Flows," *Handbook of Heat Transfer*, edited by W. M. Rohsenow and J. P. Hartnett, McGraw-Hill, New York, 1973.

[10] Schick, H. L., *Thermodynamics of Certain Refractory Compounds*, Vol. II, Academic Press, New York, 1966.

[11] Hansen, M., *Constitution of Binary Alloys*, 2nd ed., McGraw-Hill, New York, 1958.

[12] Elliott, R. P., *Constitution of Binary Alloys, First Supplement*, McGraw-Hill, New York, 1965.

[13] "Avco Hyperthermal Simulation Capabilities," Rept. AVSD-0457-70-CA, Sept. 1970, Avco Systems Division, Wilmington, Mass.

MAY 1975 AIAA JOURNAL VOL. 13, NO. 5

Vectored Injection into Laminar Boundary Layers with Heat Transfer

G. R. Inger* and T. F. Swean†

Virginia Polytechnic Institute and State University, Blacksburg, Va.

A basic theoretical investigation of self-similar isobaric laminar two-dimensional or axisymmetric boundary-layer flows is presented for a wide range of normal and tangential surface mass transfer velocities ("vectored" injection and suction) in the presence of heat transfer. Vanishingly-small skin friction conditions pertaining to incipient separation are included. A new set of double-valued solutions pertaining to the case of small-to-moderate upstream vectoring is identified and studied. Also, the frictional heating associated with vectoring is shown to have a significant effect on the heat transfer and recovery factor for high-speed flows. Detailed results are presented for skin friction, velocity and enthalpy profiles, and momentum, and displacement thickness integral properties.

Nomenclature

C_p = constant pressure specific heat
f_w = normal injection parameter
f'_w = tangential injection parameter
g_w = surface total enthalpy ratio
h, H = static and total enthalpy, respectively ($H = h + u^2/2$)
$I_0 = \int_0^\infty (g - f')\,d\eta$
$I_1 = \int_0^\infty (g - f'^2)\,d\eta$
$I_2 = \int_0^\infty f'(1-f')\,d\eta$
M = Mach number
Pr = Prandtl number
$\dot{q}_w$ = surface heat transfer rate
r_B = body radius
Re_x = Reynolds number, $\rho_e u_e x/\mu_e$
T = static temperature
u, v = velocity components in x, y coordinate directions
x, y = streamwise and normal physical coordinates
Z = recovery factor parameter (Eq. 12)
γ = ratio of specific heats
δ = boundary-layer thickness
δ^* = boundary-layer displacement thickness
ε = 0, 1 for $2-D$ and axisymetric flow, respectively

Presented as Paper 74-676 at the AIAA/ASME 1974 Thermophysics and Heat Transfer Conference, Boston, Massachusetts, July 15–17, 1974; submitted August 19, 1974; revision received October 16, 1974. Research was supported by the National Science Foundation under Grant NSF-6K20379 and by the Air Force Office of Scientific Research under Grant 72-2173.

Index category: Boundary Layers and Convective Heat Transfer—Laminar.

* Professor, Department of Aerospace and Ocean Engineering. Associate Fellow AIAA.

† Graduate Research Assistant, Department of Aerospace and Ocean Engineering.